ELSEVIER

Journal of Alloys and Compounds 434–435 (2007) 156–159

Journal of ALLOYS AND COMPOUNDS

www.elsevier.com/locate/jallcom

The effect of Zr addition in glass forming ability of Ni–Nb alloy system

H.J. Chang [a], E.S. Park [a], Y.S. Jung [a], M.K. Kim [b], D.H. Kim [a,*]

[a] *Center for Non-crystalline Materials, Department of Metallurgical Engineering, Yonsei University, 134 Shinchon-dong, Seodaemun-ku, Seoul 120-749, Republic of Korea*

[b] *Pohang Accelerator Laboratory, Beamline Department, Pohang University of Science and Technology, San 31, Hyoja-dong, Pohang 790-784, Republic of Korea*

Available online 30 October 2006

Abstract

The effect of Zr addition on glass forming ability (GFA) of Ni–Nb alloys has been investigated. $Ni_{60}Nb_{40-x}Zr_x$ ($x = 0$–40) alloys were prepared by melt-spinning and injection-casting. Crystallization behavior of the alloys was studied by differential scanning calorimetry (DSC), differential thermal analyzer (DTA) and X-ray diffractometry (XRD). The GFA increased with the addition of Zr, thus, a rod with the diameter of 2 mm was obtained in $Ni_{60}Nb_{30}Zr_{10}$ which has the highest reduced glass transition T_{rg} value of 0.619 among the alloys investigated. When Zr content is more than 10 at.%, the GFA deteriorated significantly. The atomic structure of Ni–Nb–Zr alloys investigated by means of extended X-ray absorption fine structure (EXAFS), indicated presence of chemical inhomogeneity in the amorphous structure due to the positive mixing enthalpy between Zr and Nb.

Keywords: Ni–Nb-based alloy; Bulk metallic glass; EXAFS; Chemical inhomogeneity

1. Introduction

Ni–Nb alloy is considered to be a bulk metallic glass (BMG) forming systems having potential for application since binary $Ni_{59.5}Nb_{40.5}$ alloy forms 1 mm diameter glassy rod by injection-casting [1]. The Ni–Nb glassy alloy also exhibits high compressive strength of ~3 GPa and excellent corrosion resistance [2]. In order to enhance the glass forming ability (GFA) of the Ni–Nb alloy further, effect of addition of third alloying element such as Ti, Sn and Ta, etc., has been studied [3–5]. The maximum diameter of glassy rod by injection-casting increased up to 3 mm in $Ni_{59.5}Nb_{33.6}Sn_{6.9}$ alloy [4] and compressive fracture strength higher than 3 GPa was obtained in $Ni_{60}Nb_{25}Ti_{15}$ and $Ni_{60}Nb_{30}Ta_{10}$ glassy alloys [3,5]. It has been known that addition of elements which have negative mixing enthalpy with constituent elements is favorable for enhancement of GFA based on the empirical rules [6,7]. The mixing enthalpy of Sn and Ta with Ni is −4 and −29 J/mol [8], respectively. When Ti was added into Ni–Nb alloy, the maximum diameter of the glassy rod increased to 1.5 mm and compressive strain before fracture increased by about 1.5%, in spite of positive mixing enthalpy between Ti and Nb (+2 kJ/mol) [8].

Since rapidly solidified Ni–Nb [9] and Ni–Zr [10] alloys are known to be amorphous phase over wide composition ranges, it is expected that Ni–Nb–Zr alloys would also be a good glass formers in a wide composition range. Kimura et al. showed the formation ranges of amorphous phase and thermal stability in Ni–Nb–Zr alloy system [11]. The amorphous phase forms in a wide range from 20 to 75 at.% Ni, 0 to 60 at.% Nb and 0 to 80 at.% Zr. Interestingly, Zr has a positive heat of mixing with Nb which causes solid state miscibility gap.

In the present study, the effect of addition of Zr having positive heat of mixing with Nb (+4 kJ/mol) on the GFA of Ni–Nb alloys has been investigated. $Ni_{60}Nb_{40-x}Zr_x$ ($x = 0$–40) alloys have been prepared by melt-spinning and injection-casting methods to investigate the thermal stability of the glass phase and GFA. The effect of Zr addition on the local structural change in Ni–Nb amorphous phase has been investigated using extended X-ray absorption fine structure (EXAFS) data, and the relation between local structural change and GFA has been discussed.

2. Experimental details

Multi-component Ni–Nb-based alloy ingots were prepared by arc-melting a mixture of the elements having a purity of 99.9 at.% or better under high-purity argon atmosphere. The alloyed ingots were then remelted under high

* Corresponding author. Fax: +82 2 312 8281.
E-mail address: dohkim@yonsei.ac.kr (D.H. Kim).

0925-8388/$ – see front matter © 2006 Elsevier B.V. All rights reserved.
doi:10.1016/j.jallcom.2006.08.292

vacuum in a quartz tube and were injected into a copper mold. Glassy alloys were produced in a cylindrical rod with diameters up to 2 mm. Rapidly solidified ribbon specimens were prepared by remelting the alloy ingots in quartz tubes, followed by ejecting with an over-pressure of 50 kPa through a nozzle onto a Cu wheel rotating with a surface velocity of 40 m/s. The resulting ribbons have a thickness of about 30 μm and a width of about 6 mm.

The glassy phase was identified by X-ray diffraction (XRD, Rigaku) with a collimated Cu Kα X-ray source and transmission electron microscopy (TEM, JEM 2000EX). Thermal behavior associated with glass transition (T_g), crystallization (T_x) and liquidus melting temperature (T_l) was examined with a differential scanning calorimeter (DSC, Perkin-Elmer DSC7) at heating rate of 0.67 K/s and differential thermal analyzer (DTA, Perkin-Elmer DTA7) at heating rate of 0.33 K/s. The T_g is defined as the mid-height point of the endothermic event for glass transition.

For detailed structural analysis, EXAFS data in the vicinity of the Ni K-edges, Nb K-edges of melt-spun $Ni_{60}Nb_{40-x}Zr_x$ ($x = 0$, 10 and 20) alloys were obtained using synchrotron radiation source at the BL7C1 beamline of the Pohang Light Source (2.5 GeV). Si (3 1 1) monochromator crystal was used with detuning to 70% in intensity to eliminate high-order harmonics. X-ray fluorescence photons emitted from the specimen surface were detected using an X-ray fluorescence detector (Canberra-Planar Silicon detector; PD3000). Energy calibration was carried out with the Ni, Nb and Zr foil assigning the first inflection point to 8333, 18,986 and 17,998 eV, respectively. The EXAFS data analysis was carried out by standard procedure.

3. Results

All the XRD patterns obtained from melt-spun ribbons of $Ni_{60}Nb_{40-x}Zr_x$ ($x = 0$, 5, 10, 15, 20, 25, 30, 35, 40) exhibited a series of broad diffraction maxima characteristic of amorphous phase, with no evidence of crystalline Bragg peaks (not shown here). Bright field TEM images and diffraction patterns also confirmed ribbons have a fully amorphous structure (not shown here). Fig. 1 shows (a) DSC and (b) DTA curves of the $Ni_{60}Nb_{40-x}Zr_x$ ($x = 0$, 5, 10, 15, 20, 25) alloys. The glass transition was not observed, for Zr content, $x \geq 30$ at.%. Therefore, DSC and DTA data for $x = 30$, 35, 40 were not included in Fig. 1. With Zr addition ($x = 20$), two-step crystallization behavior (two exothermic peaks) changed into one step crystallization behavior (one exothermic peak). Table 1 lists the results of thermal analysis (T_g, T_x and T_l) and parameters for GFA (supercooled liquid region, $\Delta T_x = T_x - T_g$, and reduced glass transition temperature, $T_{rg} = T_g/T_l$, K ($=[T_x - T_g]/[T_l - T_x]$) [12] and γ ($=T_x/[T_l + T_g]$) [13]). The characteristic temperatures (T_g, T_x and T_l), ΔT_x and T_{rg} values were plotted as a function of Zr content (0–25 at.%) in Fig. 2. ΔT_x increases from 33 to 38 K with increasing Zr content from $x = 0$ to 20, then decreases to 31 K with further increase to 25%. DTA data showed that T_l decreases with addition of Zr, i.e. 1478 K at $x = 0$, and 1390 K at $x = 15$. However, two endothermic melting peaks were observed for alloy $x = 5$ and 10, indicating the composition is not pseudo-eutectic. In contrast, for $x = 20$ and 25 only one endothermic melting peak appears. For $x = 10$, 15 and 20, T_g was 875, 860 and 853 K, respectively, while T_l was 1413, 1390 and 1391 K, respectively, thus, T_{rg} was 0.619, 0.619 and 0.613, respectively.

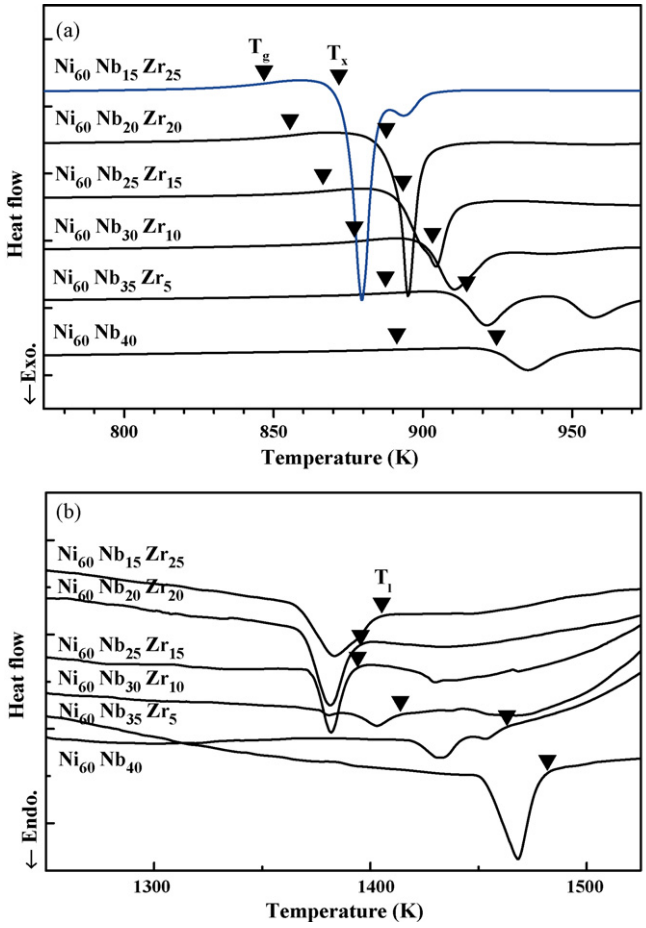

Fig. 1. (a) DSC and (b) DTA traces of the melt-spun $Ni_{60}Nb_{40-x}Zr_x$ ($x = 0$, 5, 10, 15, 20, 25).

We performed injection-casting to evaluate the GFA of the alloys. The $Ni_{60}Nb_{30}Zr_{10}$ alloy was found to have the highest GFA among the alloy investigated, enabling formation of maximum 2 mm diameter glassy rod. Fig. 3 shows DSC traces of $Ni_{60}Nb_{30}Zr_{10}$ alloy ribbon and rod with a diameter of 1 and 2 mm. T_g and T_x were 875 and 902 K, respectively, and the heat release upon devitrification was about −28 J/g in melt-spun rib-

Table 1
Results of the thermal analysis (T_g, T_x and T_l), parameters for GFA, i.e. ΔT_x, T_{rg}, K and γ parameters, and D_{max} for $Ni_{60}Nb_{40-x}Zr_x$ ($x = 0$, 5, 10, 15, 20, 25)

	T_g	T_x	T_l	ΔT_x	T_{rg}	K	γ	D_{max}
$Ni_{60}Nb_{40}$	891	924	1478	33	0.603	0.058	0.390	1
$Ni_{60}Nb_{35}Zr_5$	887	911	1458	24	0.608	0.044	0.389	1.5
$Ni_{60}Nb_{30}Zr_{10}$	875	902	1413	27	0.619	0.053	0.394	2
$Ni_{60}Nb_{25}Zr_{15}$	860	891	1390	31	0.619	0.062	0.396	1.5
$Ni_{60}Nb_{20}Zr_{20}$	853	891	1391	38	0.613	0.076	0.397	0.5
$Ni_{60}Nb_{15}Zr_{25}$	843	874	1405	31	0.600	0.058	0.389	0.1
Regression coefficient (R^2)	–	–	–	0.165	0.463	0.106	0.088	1

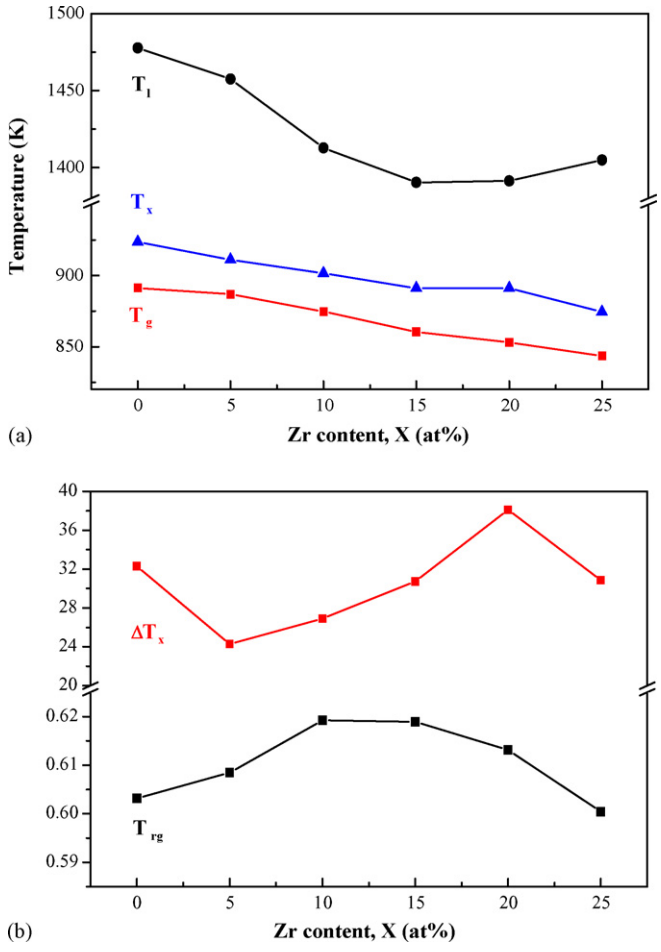

Fig. 2. (a) Thermal analysis (T_g, T_x and T_l) and (b) GFA parameters (ΔT_x and T_{rg}) for melt-spun $Ni_{60}Nb_{40-x}Zr_x$ ($x = 0$, 5, 10, 15, 20, 25).

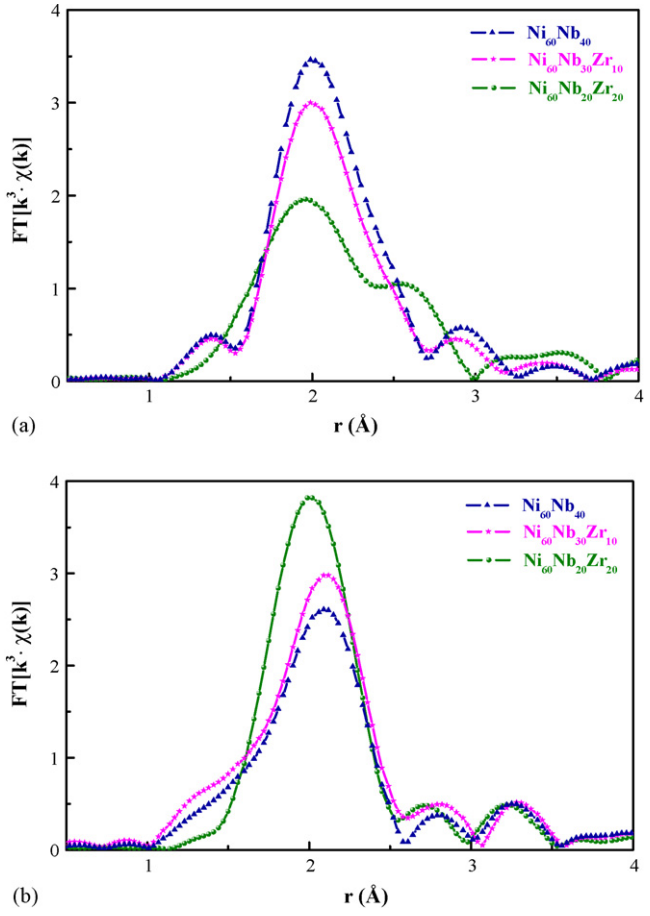

Fig. 4. Fourier transform magnitudes (FT[$k^3(k)$]) around: (a) Ni and (b) Nb for melt-spun $Ni_{60}Nb_{40-x}Zr_x$ ($x = 0$, 10 and 20) alloys.

bon and injection-cast rod (1 and 2 mm), indicating that 2 mm diameter $Ni_{60}Nb_{30}Zr_{10}$ alloy rod is fully amorphous phase. DSC traces of 3 mm $Ni_{60}Nb_{30}Zr_{10}$ alloy rod show a significant decrease of exothermic heat during crystallization, indicating that partial crystallization occurred during solidification. The present results show that maximum diameter for glass formation increased from 1 mm for the alloy $x = 0$ to 2 mm for the alloy $x = 10$. For Zr content more than 10 at.%, the GFA deteriorates.

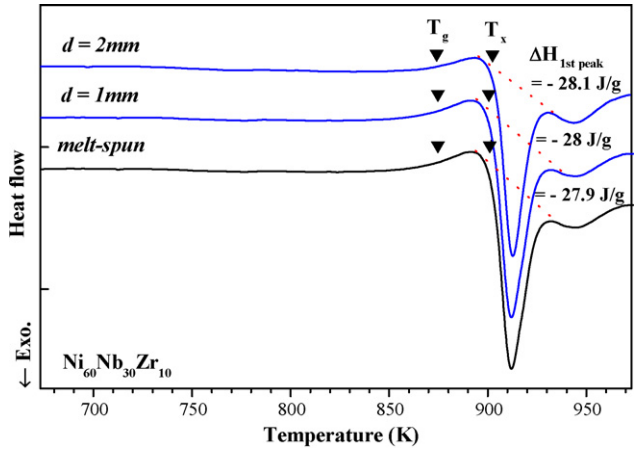

Fig. 3. DSC traces of melt-spun and injection-cast (1 and 2 mm) $Ni_{60}Nb_{30}Zr_{10}$.

Fig. 4(a and b) shows nearest neighbor distances around Ni and Nb atoms in $Ni_{60}Nb_{40-x}Zr_x$ ($x = 0$, 10 and 20) melt-spun ribbon samples. The data were obtained after background-subtraction, normalization to unit edge, interpolation to momentum space (k-space) and Fourier transformation into r-space with Hanning window for the k^3-weighted in the k range of 2–13.5 (k: wave number). Fourier transformed magnitude, FT[$k^n(k)$] is proportional to the probability of finding an atom at a given radial distance from the central atom. The distance in x-axis in Fig. 4 is unitless because the data was not fitted. The main peaks at 2–2.1 (Fig. 4(a and b)) corresponds to the nearest (first shell) Ni, Nb and Zr atoms' configuration around Ni atom and Nb atom, respectively.

When the nearest neighbor distances around Ni atom is considered (Fig. 4(a)), the intensity of the main peak at about 2 decreased with the addition of Zr. The main peak was separated into two broad peaks at 1.8 and 2.5 when Zr content was 20 at.%. In contrast, when the nearest neighbor distances around Nb atom is considered (Fig. 4(b)), the intensity of the main peak at 2.1 increased significantly with the addition of Zr. The main peak was separated into two broad peaks at 1.9 and 2.4, when Zr content was 20 at.%.

4. Discussion

Table 1 summarizes the results of the thermal analysis and maximum diameter for glass formation (D_{max}) in $Ni_{60}Nb_{40-x}Zr_x$ ($x = 0$, 5, 10, 15, 20, 25) alloys, characteristic temperatures (T_g, T_x and T_l) and parameters for GFA ΔT_x, T_{rg}, K [12] and γ [13]. Each of the parameters was proposed based on different viewpoints on glass formation, i.e. ΔT_x, stability of glass phase; T_{rg}, kinetic ability to avoid crystallization during cooling; K, relative stability of supercooled liquid; γ, stability of liquid and kinetic ability to resist crystallization. With increasing Zr content in $Ni_{60}Nb_{40-x}Zr_x$, GFA slightly increases up to $x = 10$ and then decreases with further replacement of Nb by Zr, as shown in Fig. 2(b). However, liquidus melting temperature decreases with increasing x to $x = 15$, indicating that the origin of the GFA enhancement cannot be explained clearly from the thermodynamic point of view. In order to reveal how closely the estimated values from the regression correspond to the actual experimental data, the statistical correlation parameter, R^2, was calculated and listed in Table 1. The R^2 values for T_{rg} are higher than other parameters, implying that T_{rg} shows a good correlation with D_{max} for alloys $x = 0$–25.

Presence of multiple components is an important parameter to improve the GFA based on the so-called confusion principle [14]. GFA increase in the present study can be attributed to the increase of the number of components ($2 \rightarrow 3$). It is also explained by the empirical rules: (1) large atomic size difference between the alloy elements (Ni: 1.24 Å; Nb: 1.46 Å; Zr: 1.60 Å); (2) large negative mixing enthalpy between the alloy elements (Ni–Nb: −30 J/mol; Ni–Zr: −49 J/mol) [8]. A large atomic size difference between constituent elements is favorable to increase the atomic packing density of the liquid structure, destabilizing the competing crystalline phase against the glass formation. Therefore, it becomes more difficult to satisfy the compositional requirements for the formation of nuclei with the addition of Zr. However, addition of Zr beyond 10 at.% deteriorates GFA significantly. The reason can be discussed with EXAFS data shown in Fig. 4. Since amorphous phase does not have long range ordering but random configuration, only one major peak corresponding to the first shell appears in the EXAFS data of the amorphous phase. If addition of an element (Zr) leads to an increase in the degree of dense random packed atomic configuration, rearrangement of the constituent elements on a long-range scale becomes difficult and the peak intensity in Fourier transformed magnitude decreases (Fig. 4). The decrease of peak intensity with Zr addition in Fig. 4(a) indicates increase of disorder around Ni atoms, while the increase of peak intensity with Zr addition in Fig. 4(b) indicates that Zr atom stimulates the decrease of disorder around Nb atom. The addition of 20 at.% Zr leads to separation of the main peak into two peaks, indicating that there are chemically preferred bonding like Ni–Ni and Ni–Zr around Ni atoms and Nb–Ni and Nb–Nb around Nb atom. Therefore, addition of Zr over 10 at.% leads to the chemical inhomogeniety or short range ordering (SRO) in the amorphous structure. The chemical inhomogeneity is connected with positive heat of mixing between Nb and Zr, which causes miscibility gap in the Nb–Zr binary system. This atomic structural change may be able to affect the GFA. Therefore, the present study shows that if addition of element causes chemical inhomogeneity in the amorphous structure, the GFA deteriorates. This may explain why the GFA decreases when Zr addition (x) is over 10 at.% in $Ni_{60}Nb_{40-x}Zr_x$ alloy.

5. Conclusions

We have synthesized bulk metallic glasses to examine the enhancement of GFA in Ni–Nb system by the addition of Zr. The maximum diameter of glassy rod that can be fabricated is about 2 mm for $Ni_{60}Nb_{30}Zr_{10}$ exhibiting the largest T_{rg} value of 0.619. Although the R^2 values for T_{rg} are higher than other parameters suggested so far, only thermodynamic and/or kinetic criteria for GFA (ΔT_x, T_{rg}, K and γ parameters) are not sufficient for evaluating the GFA of Ni–Nb–Zr alloy system.

The reason that addition of Zr beyond 10 at.% deteriorates the GFA significantly can be discussed with EXAFS data. EXAFS data shows that there is an evidence of local short range ordering or chemical inhomogeniety caused by the preferential chemical bonding when amount of Zr is over 10 at.%. This chemical inhomogeniety can lead to the decrease of the GFA of Ni–Nb–Zr alloy.

Acknowledgements

This work was supported by the Creative Research Initiatives of the Korean Ministry of Science and Technology. We are grateful to authorities concerned of Pohang Light Source (PLS) for XAS measurements.

References

[1] M. Leongardt, W. Loser, H.-G. Lindenkreuz, Acta Mater. 47 (1999) 2961.
[2] A. Kawashima, H. Habazaki, K. Hashimoto, Mater. Sci. Eng. A 304–306 (2001) 753.
[3] W. Zhang, A. Inoue, Mater. Trans. 43 (9) (2002) 2342.
[4] H. Choi-Yim, D. Xu, W.L. Johnson, Appl. Phys. Lett. 82 (7) (2003) 1030.
[5] M.H. Lee, D.H. Bae, W.T. Kim, D.H. Kim, Mater. Trans. 44 (10) (2003) 2084.
[6] A. Inoue, Acta Mater. 48 (2000) 279.
[7] E.S. Park, D.H. Kim, Mater. Met. Int. 11 (2005) 19.
[8] F.R. Niessen, Cohesion in Metals, Elsevier B.V. Science Publishers, Amsterdam, 1988.
[9] R.C. Rhul, B.C. Giessen, M. Cohen, N.J. Grant, Acta Metall. 15 (1967) 1693.
[10] K.H.J. Buschow, N.M. Beekmans, Phys. Rev. B 19 (1979) 3843.
[11] H. Kimura, A. Inoue, S. Yamaura, K. Sasamori, M. Nishida, Y. Shinpo, H. Okouchi, Mater. Trans. 44 (6) (2003) 1167.
[12] A. Hruby, Czech. J. Phys. B 22 (1972) 1187.
[13] Z.P. Lu, C.T. Liu, Acta Mater. 50 (2002) 3501.
[14] A.L. Greer, Nature 366 (1993) 303.